https://ntrs.nasa.gov/search.jsp?R=20060020181 2019-08-29T21:57:04+00:00Z

Planar laser-induced fluorescence (PLIF) investigation of hypersonic flowfields in a Mach 10 wind tunnel (invited)

P.M. Danehy[*], J.A. Wilkes[†], D.W. Alderfer[‡], S.B. Jones[§], A.W. Robbins[**]
NASA Langley Research Center, Hampton VA, 23681-2199

D. P. Patry[††] and R. J. Schwartz[‡‡]
Swales Aerospace, Hampton VA, 23681-2199

Planar laser-induced fluorescence (PLIF) of nitric oxide (NO) was used to visualize four different hypersonic flowfields in the NASA Langley Research Center 31-Inch Mach 10 Air wind tunnel. The four configurations were: (1) the wake flowfield of a fuselage-only X-33 lifting body, (2) flow over a flat plate containing a rectangular cavity, (3) flow over a 70° blunted cone with a cylindrical afterbody, formerly studied by an AGARD working group, and (4) an Apollo-geometry entry capsule – relevant to the Crew Exploration Vehicle currently being developed by NASA. In all cases, NO was seeded into the flowfield through tubes inside or attached to the model sting and strut. PLIF was used to visualize the NO in the flowfield. In some cases pure NO was seeded into the flow while in other cases a 5% NO, 95% N_2 mix was injected. Several parameters were varied including seeding method and location, seeding mass flow rate, model angle of attack and tunnel stagnation pressure, which varies the unit Reynolds number. The location of the laser sheet was as also varied to provide three dimensional flow information. Virtual Diagnostics Interface (ViDI) technology developed at NASA Langley was used to visualize the data sets in post processing. The measurements demonstrate some of the capabilities of the PLIF method for studying hypersonic flows.

I. Introduction

Visualization of hypersonic flow has traditionally been performed using the shadowgraph and schlieren methods. A collimated beam of white light is typically directed across the hypersonic flow and is refracted by density variations (such as shock and expansion waves) in the flow. The light is imaged by a lens or mirror onto a screen or camera, resulting in shadows where sharp density gradients appear in the flow (shadowgraph), or else a knife edge is used to enhance this effect by blocking some of the higher frequency spatial information (schlieren). Both techniques allow shock and expansion waves, as well as turbulent flow, to be visualized. These methods are relatively simple and inexpensive to implement: they require optical access but do not require advanced laser technology. These visualization methods have been used successfully for decades and have aided in many advancements in the field of hypersonics.

Shadowgraph and schlieren, however, have several limitations. Both are path-integrated measurements. Thus, measurements are averaged along the line of sight of the light beam so that three dimensional flow features are not resolved. The so-called "focusing schleiren" method[1] partially overcomes this limitation, but with degraded image quality and the spatial resolution along the line of sight tends to be on the order of a few centimeters. Also, shadowgraph and schlieren generally cannot visualize flows in cavities or corners, such as a wing-body junction on a test article because the model obscures the view. Another drawback in some situations is that shadowgraph and

[*] Research Scientist, Advanced Sensing and Optical Measurement Branch, MS 493, AIAA Associate Fellow.
[†] PhD Student, Department of Physics, College of William and Mary, Williamsburg ,VA and NASA Graduate Co-op Student, Advanced Sensing and Optical Measurement Branch, MS 493, AIAA Student Member.
[‡] Research Scientist, Advanced Sensing and Optical Measurement Branch, MS 493
[§] Optic and Electronic Technician, Advanced Sensing and Optical Measurement Branch, MS 493
[**] Mechanical Technician,
[††] Information Technology Specialist, MS 493, NASA Langley Research Center.
[‡‡] Senior Research Engineer, MS 493, NASA Langley Research Center

schlieren are insensitive to gas composition. Furthermore, shadowgraph and schlieren lack sufficient sensitivity to resolve weak density gradients in low density flows, such as those that may occur for hypersonic wake flows. Finally, shadowgraph and schlieren are generally not quantitative, other than for determining the shapes of features like shock and expansion waves.

Various planar imaging techniques have been used to study hypersonic flows, most notably Planar Rayleigh Scattering (PRS)[2] and planar laser-induced fluorescence (PLIF). These flow-imaging techniques overcome many of the limitations of shadowgraph and schlieren. While PRS involves elastic scattering from molecules, PLIF electronically excites certain molecules in the flow. In both cases, a planar laser sheet is directed into the flow and the interrogated molecules scatter or emit light which is collected using a lens and CCD camera that is typically oriented to view the light sheet perpendicularly. The spatial resolution for these planar imaging techniques is determined by the thickness of the laser sheet (generally $\leq$1 mm) and the resolution and magnification of the camera/lens system (typically 0.05 to 1 mm/pixel). These planar imaging methods can be used to investigate cavity and corner flows as well as highly three dimensional flows with adequate spatial resolution to resolve the dominant flow structures.

PLIF requires the presence of an atom or molecule, such as nitric oxide (NO) that can absorb laser light and emit it as fluorescence. This can be an advantage for visualizing gas jets, such as Reaction Control System (RCS) jets where the tracer molecule allows the jet fluid to be clearly distinguished from the ambient fluid.[3] But it is also a limitation since NO or some other tracer molecule must be present in or added to the flowfield to use this method. PRS on the other hand, has a significant advantage in that all molecules elastically scatter light, so PRS could potentially be used in any flow. However, the intensity of Rayleigh scattering is proportional to the gas density. In many hypersonic flowfields the densities are relatively low and so are the PRS signal intensities. The PLIF signal intensity is insensitive to pressure over a range of low pressures, so it is more suitable for probing low-density hypersonic flowfields than PRS. Another significant advantage of PLIF is that the fluorescence is usually detected at a wavelength shifted several tens of nanometers from the excitation wavelength. Thus, light scattered from the surface of the model, from particles in the flow and from the tunnel walls can be suppressed using optical filters. PLIF and PRS can both be used for quantitative measurement of thermodynamic parameters, including temperature and velocity.

In this paper, we use planar laser-induced fluorescence of nitric oxide to visualize four different hypersonic flowfields. The NO PLIF method has been successfully applied in a variety of supersonic and hypersonic flow facilities.[4,5,6,7,8,9,10,11,12] Also, PLIF of I_2 has previously been performed in a hypersonic wind tunnel at NASA Langley Research Center[13] and elsewhere[14]. Based on these promising results, a portable NO PLIF system[15] was constructed at NASA Langley Research Center. While this system has been used extensively in a vacuum chamber at NASA Langley Research Center to test free and impinging low-Reynolds number jets[16] for the Space Shuttle Return-To-Flight (RTF) Program, this was the first entry of this system in a hypersonic wind tunnel under normal operation. The main goal of the test was to demonstrate the capabilities of the PLIF system and to prove its applicability to a variety of flowfields of interest to hypersonics researchers. All of the experiments were performed in the NASA Langley Research Center 31-Inch Mach 10 Air wind tunnel in April and May 2005. Four configurations were investigated:

(1) The wake flowfield of a fuselage-only X-33 model. This model was chosen because it had suitable internal plumbing and was representative of a lifting body;

(2) Flow over and into a rectangular cavity mounted in a flat plate having a sharp leading edge. This model was chosen due to its applicability to a missing Space Shuttle Orbiter heat shield tile, or a heat shield damage site. It is also representative of hypersonic store separation relevant to military applications;

(3) Flow over a planetary entry forebody shape: a 70 degree cone with a spherical nose – similar to the Viking aeroshell used for most Mars entries. This model was probed because of a desire to demonstrate the ability to visualize and distinguish between laminar and turbulent wake flows in planetary entry configurations;

(4) Flow over an Apollo-geometry entry capsule. This configuration was chosen because it was expected that the new Crew Exploration Vehicle would be a capsule. Two main efforts were undertaken in these entry capsule tests: (i) efforts were made to seed the forebody, shear layer, and separated wake flows with NO to allow flow visualization without perturbing the flow and (ii) an RCS jet was seeded with NO and visualized. A previous paper[3] detailed the PLIF measurements performed in the RCS jet; these results will only be summarized briefly here. The other Apollo-geometry experiments are reported herein for the first time.

II. Experimental Description

The experiments were performed in the 31-Inch Mach 10 Air wind tunnel at the NASA Langley Research Center. The test apparatus consisted of three main components: the test models, the wind tunnel facility and the optical visualization systems, which are detailed below.

A. Model Geometries

(1) X-33 Model. The X-33 vehicle was developed for NASA by Lockheed Martin between 1996 and 2001. The vehicle had a lifting-body delta planform, with twin vertical tails, two canted fins, and two body flaps. It was to be powered by two linear aerospike engines.[17] One goal of the PLIF test reported in this paper was to demonstrate the ability to measure lifting body wake flows generated by vehicles like the Space Shuttle Orbiter and X-33. A suitable Shuttle Orbiter model was not available, but an X-33 model containing stainless steel tubes plumbed to the model surface was available. These tubes would normally be used to measure the model surface pressure, but NO could also be supplied through these tubes to locally seed the flowfield. The many connected tubes allowed delivery of NO at various places on the model including the stagnation point on the nose of the model. The X-33 model available for the current study lacked both the canted fins and the body flaps ordinarily present on the X-33; it had been created for a series of tests designed to use measured surface pressures to explain differences between the pitching moments that had been previously been measured in the 20-Inch Mach 6 and the 31-Inch Mach 10 wind tunnels using a different model.[18] The model was a 0.007-scale fuselage-only model was also designed and fabricated in-house at LaRC based on the X-33 604B0002G configuration.[18] It was 100.0 mm wide at the base was about 130 mm long. The model had 20 static pressure ports which consisted of stainless steel tubes plumbed out of the test section through the sting. Some tubes were used in the present experiment to deliver NO into the flow. The 10 pressure orifices on the windward side were 0.030-in diameter and the 10 on the leeward side were 0.060-in diameter. The model was mounted to a blade mount such that the nose of the model was approximately in line with the axis of the main supporting strut and the model was at an angle of attack (AoA) of 30° when the sting angle was 0°. See Reference 18 for further details on this model. The model AoA was varied from 30° to 45° during testing.

(2) Flat plate flow with a cavity. A flat plate was mounted on a wedge-shaped model having a sharp leading edge. The wedge half angle was 10°. Thus a 0° sting angle corresponded to a -10° angle of attack for the flat plate. The flat plate was 127.0 mm wide and 157.2 mm long. The front edge of the cavity was 81.0 mm downstream of the leading edge of the flat plate. The cavity was 40.14 mm long and 10.13 mm wide. The depth of the cavity was 7.96 mm, although 5.23 mm below the surface, the length and width abruptly decreased to 38.52 by 8.53 mm. The dimensions of the cavity reported here were measured with an accuracy of ±0.03 mm. There was no floor on the cavity. That is, the cavity was open to the internal volume of the wedge model which was an odd shaped volume of about 150 cubic centimeters. Tubes ran from the sting through this volume to the pressure ports as well as to four NO seeding ports on the model centerline. NO was plumbed through a mass flow controller into a manifold that split the NO equally between these four ports. A mass flow rate of 0.100 slpm (standard liters per minute) of pure NO was used for the test, resulting in ~0.025 slpm of NO per port. The inside diameter of the ports was 0.070 in. We estimate that, for these conditions (T_0 = 1000 K, P_0 = 4.96 MPa (720 psia)), the velocity of the gas exiting the ports was about 20 m/s whereas the freestream flow velocity was 1,343 m/s. This relatively low flowrate was chosen to minimize perturbation to the flowfield while still providing good flow visualization. This flowrate of NO did not force the flow to undergo transition to turbulence either in the presence or absence of the cavity.

(3) 70° Blunted Cone with Cylindrical Afterbody. The blunted cone model had a diameter of 101.5 mm. It had a planar afterbody that was attached to a 25.5 mm diameter cylindrical sting. The sting was built with a long cavity in which a quartz window was inserted to allow an ultraviolet laser beam to pass through the sting, thereby reducing scattered light from the sting while also allowing visualization on both top and bottom of the sting. The top of the quartz window was flat while the bottom of the window was contoured to match the radius of the sting. The window was 152 mm long, 12.1 thick and its height matched the sting diameter. The angle of attack of the model was set to zero for this test. A stainless steel tube with 3.2 mm outer diameter was attached to the outside of the sting to deliver the NO through a small porous plug located 12 mm downstream of the base of the model.

(4) Apollo-Geometry Entry Capsule. The model design was based on the Apollo capsule geometry. The heat shield radius was 1.2 times the 101.6 mm diameter, the corner radius was 0.05 times the diameter, and the backshell angle was 33 degrees. The model was attached to a sting at a 28º angle, which was approximately the entry angle of attack of Apollo. Ten pressure orifices (limited in number by the inside diameter of the sting) were placed on the model to measure model pressures but also to offer different seeding locations for the NO PLIF system. In addition to standard surface orifices, an RCS plug and a porous plug were included on each side of the model. The RCS plugs incorporated a conical nozzle with an exit Mach number of 2.94. The porous plugs consisted of a sintered metal 6.3

mm in diameter to diffuse the NO flow so as to not disturb the local flow. The porous plugs were recessed from the surface of the model by 1.7 mm.

B. Planar laser-induced fluorescence (PLIF) Imaging System

The PLIF system consists primarily of the laser system, beam forming optics and the detection system. The laser system has three main components: a pump laser, a tunable pulsed dye laser (Spectra Physics PDL-2), and a wavelength extender (Spectra Physics WEX). An injection-seeded Nd:YAG laser (Spectra Physics Pro-230-10) operating at 10 Hz pumps the PDL which contained a mixture of Rhodamine 590 and Rhodamine 610 laser dyes in a methanol solvent. The output of the dye laser and the residual infrared from the Nd:YAG are combined in a WEX containing both a doubling and a mixing crystal. The resulting output is tuned to a wavelength of 226.256 nm, chosen to excite the strongly fluorescing spectral lines of NO near the Q_1 branch head.

A monitoring gas cell system is used to ensure that the laser is tuned to the correct spectral line of NO. The gas cell contains a low-pressure mixture of 5% NO in N_2. A quartz window serves as a beam splitter and sends a small portion of the laser energy through windows on either side of the gas cell. A photomultiplier tube (PMT) monitors the fluorescence intensity through a third window at right angles to the path of the laser beam.

The components of this laser system are mounted within a two-level, enclosable, portable cart. A photograph of this portable PLIF system is shown in Fig. 1 with the panels removed to show the internal components. When all of the panels are in place, a single monochromatic ultraviolet laser beam exits the cart, creating a relatively safe operating environment. Further details of the system can be found in Reference 15.

For the experiments reported herein, this portable system was installed adjacent to the NASA Langley Research Center 31-Inch Mach 10 Air wind tunnel. A dedicated, adjustable scaffolding with attached mirrors and prisms directed the UV laser beam to the top of the wind tunnel test section. Optics then formed the beam into a 100-200 mm wide by ~1 mm thick laser sheet, which was directed vertically downward through a window in the top of the test section. The section of scaffolding directly above the test section was mounted to a translation stage that could be remotely controlled so that the laser sheet could be swept spanwise through the flowfield during a tunnel run. This was used for alignment of the laser sheet and also for scanning the image plane through the flowfield to visualize three-dimensional flow structures. The resulting fluorescence from NO molecules in the flow was imaged onto a gated, intensified CCD camera at a viewing angle normal to the laser sheet. A 1-, 2- or 3-mm thick Schott glass UG-5 filter was placed in front of the camera lens in order to attenuate scattered light at the laser emission frequency. This was particularly important when the laser sheet impinged on the model surface, potentially resulting in direct reflections towards the camera.

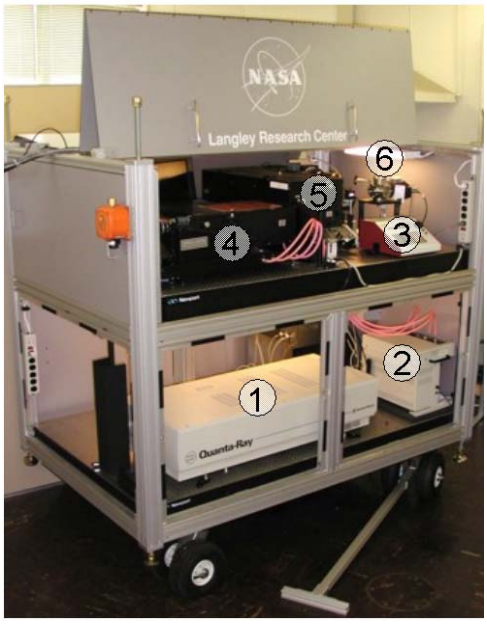

Figure 1. The portable PLIF system, shown with panels removed. Components include: (1) Nd:YAG laser; (2) dye circulators; (3) wavelength controller for the (4) pulsed dye laser; (5) wavelength extender; and (6) low-pressure monitoring gas cell.

Flow visualization images were acquired at 10 Hz with a 1 μs camera gate and a spatial resolution of approximately 2 to 7 pixels/mm, varying from run to run as different camera views and laser sheet orientations were used. An image of a scale was obtained with the PLIF camera for most of the different camera placements so that the magnification could be determined in post-processing. The temporal and spatial resolution was more than sufficient to resolve flow structures of interest.

C. Wind Tunnel, Operating Conditions, Mass Flow Control and Data Acquisition Systems

The 31-Inch Mach 10 Air wind tunnel is an electrically-heated blowdown facility located at NASA Langley Research Center in Hampton, Virginia, USA. Reference 19 details this facility, a summary of which is provided here. As the name implies, the facility has a nominal Mach number of 10 and a 31-inch square test section. The tunnel uses heated, dried, and filtered air as the test gas. The air flows from the high pressure heater, through the settling chamber, three-dimensional contoured nozzle, test section, second minimum, aftercooler and into vacuum spheres pumped by a steam ejector and conventional vacuum pumps. The test section is "closed," as opposed to an

"open jet" test section. Large windows form three walls (including top and bottom) of the test section with the fourth wall formed by the model injection system. This window arrangement has advantages in the present experiment because the laser sheet can be directed into the test section from the top window and fluorescence can be detected from the side. Also, the CCD camera can be placed very close to the test section windows, resulting in a working distance slightly larger than half of the test section width, allowing good-magnification (7 pixels/mm) PLIF images to be obtained without modification of the tunnel and without using exotic camera optics. Furthermore, the tunnel was already equipped with windows composed of UV-grade fused silica, providing ~90% transmission at the 225 nm and higher wavelengths required for PLIF.

Test durations of up to two minutes are possible in this facility. Tests could be performed approximately once per hour. The facility stagnation pressure P_0 can be varied from 350 psia (2.41 MPa) to 1450 psia (10.0 MPa) to simulate a range of Reynolds numbers.[19] Three different stagnation pressures were used in this experiment: 350 psia (2.41 MPa), 720 psia (4.96 MPa), and 1450 psia (10.0 MPa), corresponding to freestream unit Reynolds numbers of 0.5, 1.0 and 2.0 million per foot (1.64, 3.28 and 6.56 million per meter), respectively. The test core size varies from about 10 in. x 10 in. (0.25 m x 0.25 m) at the lowest stagnation pressure to 12 in. x 12 in. (0.3 m x 0.3 m) at the highest pressure.[19] The nominal stagnation temperature was 1800° Rankine (1000 K) for the experiment described herein. The freestream temperatures are estimated to be between 90° and 95° Rankine (50 and 53 K), depending on chosen operating conditions.[19] The freestream velocity is estimated to be about 4640 ft/s (1414 m/s).[19] The freestream pressure was estimated to be 0.0099 psia (68 Pa) for the P_o = 2.41 MPa (350 psia) condition, 0.0187 psia (129 Pa) for the P_o = 4.96 MPa (720 psia) condition and 0.0351 pisa (242 Pa) for the P_o = 10.0 MPa (1450 psia) condition.[19] Model surface pressures were recorded using electronically scanned pressure (ESP) piezoresistive silicon sensors connected through 4 foot long tubes to the model, though no pressure measurements are reported in this paper. This length contributed to a delayed time response. The 10-inch water column (0.36 psia) ESP module was enclosed in the tunnel injection box and thus out of the airstream. The reference side of the module was held at a low vacuum pressure. Facility and model temperatures, pressures, angles of attack, etc. were recorded by a data acquisition system at a rate of 20 Hz.

The 31-Inch Mach 10 Air wind tunnel facility was not equipped with a toxic gas cabinet for handling gas bottles containing nitric oxide (NO). Since this was a proof-of-concept study, a safe but inefficient method was used to supply NO. A small (~0.5 liter; ~17 fluid oz) vessel was pressurized with a 95% N_2, 5% NO mixture or pure NO to ~100 psia (~700 kPa). This small volume and fill pressure was used to minimize the quantity of NO gas that would have been present in the room in the event of a leak. The gas bottle needed to be refilled after 3-5 tunnel runs. The NO flowed through mass flow controllers and then through the sting and into the model through stainless steel tubing embedded in the model. This tubing connected to the port or ports where the NO would be injected. The mass flow controllers were made by Teledyne Hastings; the primary controller used in this experiment had a maximum flowrate of 1 standard liter per minute (slpm) and an accuracy of ±(0.2% of full scale + 0.5% of reading), or about 0.005 slpm for the conditions used. Nominal flowrates used in this experiment were 0.5, 0.2, 0.1, and 0.05 slpm. The flowrates were recorded by the data acquisition system at 20 Hz.

The normal sequence of operation was to begin flowing the NO mixture, then to begin the tunnel flow and wait until both flows stabilized; then the data acquisition was started, the model was injected into the flow and the camera acquisition was started (sometimes more than once per run). A manual trigger indicated to the data acquisition system that the PLIF image acquisition had begun.

III. Analysis Methods

A. PLIF Flow Visualization Image Processing

Single-shot PLIF images were processed using smoothing and by adding false color tables, but the spatial variations in laser sheet intensity were not corrected. Single-shot images were smoothed with a two-dimensional low-pass filter (MATLAB®'s "fspecial", "Gaussian" or "average" filters) prior to additional processing in order to reduce noise in the images. Averaged images were created from single-shot images that were not smoothed. These images were then made into bitmap images or movies for display on the model using the Virtual Diagnostics Interface (ViDI) described below.

It is often desirable to visualize the flow in planes other than along the flow centerline. Specifically, flow visualization in spanwise planes is often desired. In order to position the camera so that it is normal to a spanwise laser sheet, the camera would have to be in the flow of the wind tunnel, looking upstream or downstream. As this is not physically possible, two alternate approaches are used. The first approach involves positioning the camera as far upstream or downstream as optical access will allow. This results in the camera being non-normal to the plane of the laser sheet. Images acquired using this approach will include perspective distortions and, depending on the

depth-of-field of the imaging optics, the data on the edges of the image may be out of focus (although a Scheimpflug mount could be used to counteract this effect if necessary). The images shown in Fig. 2 were acquired using this approach.

The second approach involves constructing spanwise data planes from data acquired in streamwise planes via image processing. In this approach, the laser sheet is oriented parallel to the wind tunnel flow, and the camera is positioned perpendicular to the laser sheet. A translation stage is then used to translate the beam-steering and sheet-forming optics (and thus, the laser sheet) in the spanwise direction—toward or away from the camera—during a run. Images were then processed in MATLAB® to build up images in spanwise planes from the streamwise data planes. The resolution in the spanwise direction of the resulting images is determined by the original number of images that were acquired and by the physical distance over which the laser sheet was translated during the run. For example, if 100 images were acquired (corresponding to a 10-second run at a 10 Hz acquisition rate) as the laser sheet was translated 50 mm, the resulting spanwise images would be 100 pixels wide and have a 2 pixels/mm horizontal spatial resolution. This approach was used during the Apollo-geometry tests, and results are discussed in more detail below.

B. Virtual Diagnostics Interface (ViDI)

The Virtual Diagnostics Interface (ViDI)[20] is a software package developed at NASA Langley Research Center that provides unified data handling and interactive 3D display of experimental and theoretical data. Currently this technology is applied to three main areas: 1) pre-test planning and optimization; 2) analysis and comparative evaluation of experimental and computational data in near real time or in post-processing; and 3) establishment of a central hub to visualize, store and retrieve experimental results. ViDI is a combination of custom applications and the 3D commercial software Autodesk® 3ds Max®.[21]

For this experiment, ViDI was used for post-test visualization of the PLIF data. CAD (Computer Aided Design) files containing the geometry for each wind tunnel model tested were imported into the virtual environment along with the PLIF images. The PLIF images were then scaled and placed about the virtual models in positions representative of where the actual data were taken. To create the final output, a virtual camera was placed in the scene, and high resolution bitmaps were rendered. In addition, a sequential series of files containing PLIF imagery was imported to create animations of time-varying data.

IV. Results

A. Overview of the test campaign

These tests took place during a 28 calendar day interval in April and May 2005. During this time 53 tunnel runs were performed in 14 days of testing, averaging 3.8 runs per day of testing. The other calendar days or fractions of days were lost to weekends, 4 major model changes, various meetings, facility maintenance, safety checks and steam outages. Testing in the 31" Mach 10 Air tunnel without the use of PLIF typically achieves ~8 runs per day during production testing, depending on the number of model changes and the operating conditions being used. Thus the use of PLIF decreased the efficiency of testing notably. The lower operating rate when PLIF was being used is associated with additional time between runs for setting up the PLIF system for the next run. For example, changing the position and/or orientation of the laser sheet, attaching a card to the model and injecting it into the tunnel to focus the camera, waiting for the laser to warm up at the beginning of the day, etc. During this test, 9 of the 14 days of testing focused on the Apollo-geometry model. The bulk of the Apollo-geometry model testing involved visualization of RCS jets, which was detailed in Reference 3 and is only briefly summarized below. The results for all four models tested during this entry are summarized below, concluding with the Apollo-geometry tests, including notable successful tests that were not described in Reference 3.

B. Fluid Mechanical Results

(1) X-33 Model

Figure 2 shows ViDI renderings of the wake flowfield visualized by PLIF in the Mach 10 Air tunnel with the tunnel stagnation pressure equal to P_0 = 4.96 MPa (720 psia). Pure NO was seeded from the stagnation point on the nose of the X-33 model at a low flowrate of 0.1 slpm. This NO mixes into the air passing over the model and marks the fluid downstream. For each image, approximately 130 single-shot images were averaged to improve the signal-to-noise ratio. The visualization clearly shows the symmetric, upside-down-mushroom shaped vortices expected in this flow, shown most clearly in Figure 2(b). In Figures 2(c) and (d), less NO appears to be passing over the top of the model since the NO seeding port may be below the true stagnation point of the model at these angles of attack. The signal-to-noise ratio is the best in the highest angle of attack measured: 45 degrees, in Figure 2(a). However, an unexpected flow pattern was observed at high angles of attack. In Fig. 2(a) the wake vortex is asymmetric. It is skewed to one side of the model. As the angle of attack of the model was increasing, this shift in the vortices took place suddenly at AoA = 43.7°±1°. Over hundreds of images above this AoA, the vortices were never observed to switch back to the symmetric flow pattern, nor did the vortices invert to asymmetric flow on the other side of the model. Thus, the phenomenon observed is not vortex shedding. The position of the vortex pair did exhibit hysteresis: as the angle of attack was decreased, the vortices switched from asymmetric to symmetric at an AoA of 40.3°±1°, which was 3.4° lower than when ascending in AoA.

The gas pressure was measured about 20 locations including two leeward orifices located at the same downstream location but opposite spanwise sides of the model. At the 45° angle of attack these pressure ports produced nearly identical pressures. Thus, the pressure data did not sense the change in vortex pattern. It is possible that the model had been installed at a slight angle, inducing some yaw which might explain the asymmetric vortices. Or it is possible that the model was installed correctly but that the angle of attack system imparted some yaw at high angles of attack. Since this was simply a proof-of-concept test, this point was not investigated further. Had this been a typical production test, the PLIF would have indicated to the researchers that something was wrong and the model would have been checked, re-aligned and the angle of attack system tested.

For the data shown in Fig. 2, the PLIF camera was oriented at a steep angle (~30 degrees) to the laser sheet. This resulted in a significant compression of the image in one direction as well as keystone-shaped distortion. Processing an image of a square carefully drawn on a card, acquired prior to performing the experiment, allowed the nonuniform scale factor to be corrected. But the image distortions were not corrected. Thus, the images had to be rotated (a few degrees) and readjusted slightly (a few mm) to make them line up with the model in each ViDI rendering shown. Acquisition of an image of a card having a grid of uniformly spaced dots in the image plane before or after each configuration change, as

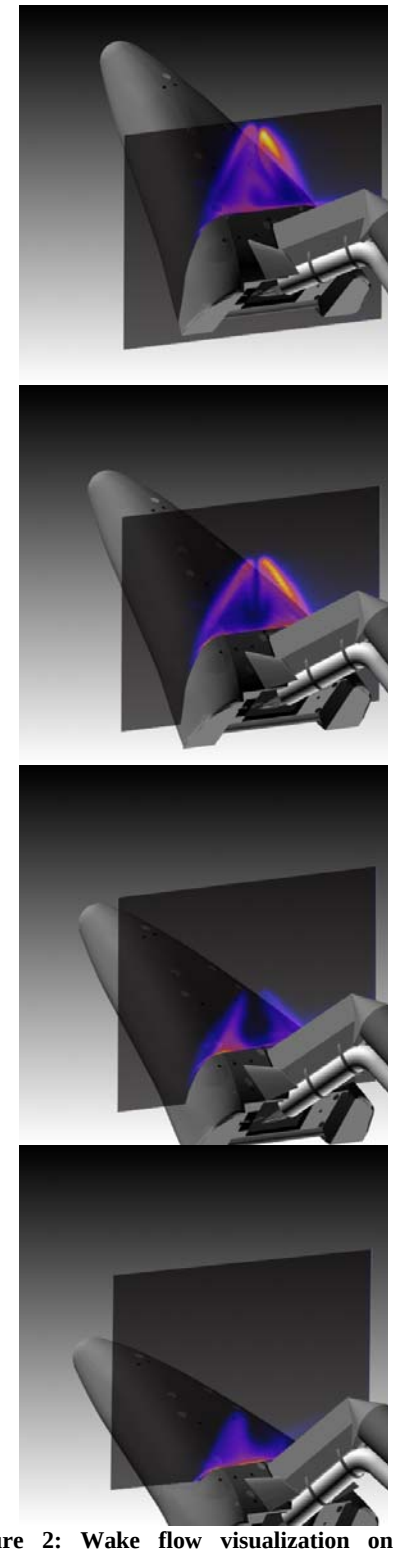

Figure 2: Wake flow visualization on a wingless X-33 configuration at Mach 10 for angles of attack of (a) 45°, (b) 40°, (c) 35° and (d) 30°.

recommended in Reference 3, would allow both of these image corrections to be made automatically and systematically in the future.

The main goal of this test was to demonstrate that the wake flowfield of a hypersonic lifting body could be visualized in the wind tunnel. Another goal of the test was to seed the flowfield without perturbing it. In a few runs with this model (not shown) several leeward side pressure ports were seeded with pure NO and PLIF was used to visualize the resulting flowfield. However, due to the low pressures on this leeward side, flow from these ports created several visible jets of NO emitting from the surface, possibly influencing the flow. Seeding the flow near the vehicle's stagnation point (on the nose) with a low flowrate of NO (0.1 slpm), may have locally perturbed the flow at that location. But the flow structures downstream showed no sensitivity to low flowrates in the range of 0 to 0.2 slpm. Also when the flowrate was doubled, the pressures measured on both the top and bottom surfaces of the model showed no measurable change, indicating that the seeded NO did not influence surface pressures.

(2) Flat Plate / Cavity Flow

Laminar hypersonic flow over a flat plate has been studied extensively by many researchers over several decades. Recently, the PLIF technique was used for measuring temperature and velocity profiles in laminar hypersonic boundary layers by O'Byrne et al.[22] The flow over rectangular cavities embedded in flat plates is an important problem for military store-separation but has gained renewed interest at NASA because of the desire to simulate the flow over the shuttle orbiter heat shield if a shuttle tile is missing or if a debris impact creates a damage site Several experiments (see Reference 23 and references therein) have recently been performed to provide data for comparison with computational simulations of these complicated flows.

In the literature (see Reference 23 for a thorough review) hypersonic cavity flows are characterized as "open", "transitional" or "closed", based on the ratio of the length, L, of the cavity to the depth, H. In open cavities, typically having $1 < L/H < 10$, the flow skips over the cavity without attaching to the floor of the cavity. In closed cavities, typically having $L/H > 14$, the flow attaches to the floor while inside the cavity. For $10<L/H<14$, the flow is usually unsteady, transitioning between opened and closed behavior. Note that flows with $L/H<1$ are considered "gaps". Another parameter of interest is the relative thickness of the boundary layer, δ, relative to H. For the present experiment, the cavity did not have a floor. Rather the cavity was open on the bottom to a hollow space nearly as deep as the cavity was long. Thus, $L/H \sim 1.5$ and the cavity would be considered open. The laminar boundary layer thickness, estimated to be between 2 and 5 mm, depending on the angle of attack, is much less than H. Thus, anticipated behavior is that the gas should skip over the cavity since it is an open cavity.

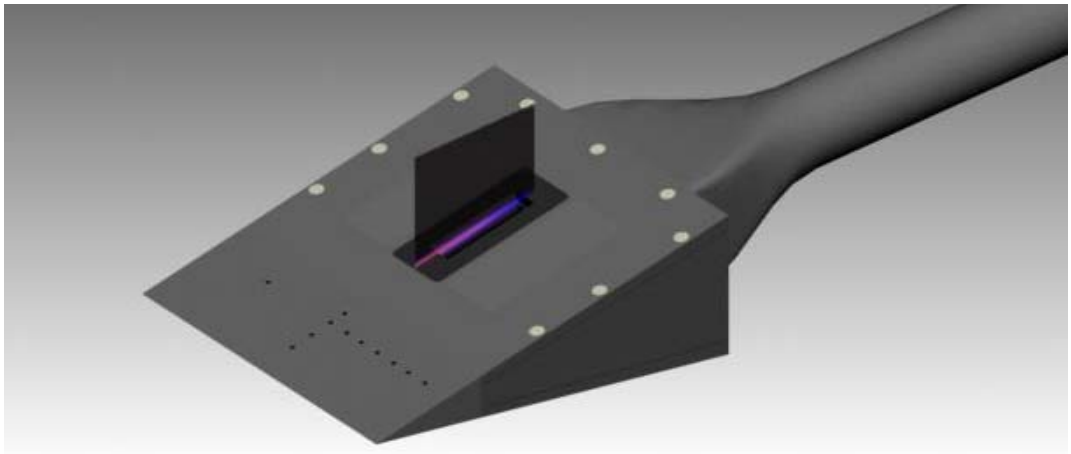

Figure 3: ViDI rendering of the flat plate / cavity flow experiment: zoomed out view.

Figure 3 shows a ViDI rendering of the test article with a plane of data superimposed. The vertical black shaded area indicates the imaged region. Flow is from bottom left to top right. The dark holes near the sharp leading edge are pressure ports and fluid injection ports. NO was injected from the four ports in a row on the model centerline. The white dots around the sides and back of the flat plate are screw holes that were filled with plaster to make them smooth. The metal surrounding the cavity was colored black with a permanent marker in the experiment to reduce glare and reflected fluorescence.

Figures 4(a) and (b) show zoomed in views of the flow near the cavity. The NO seeded into the freestream has been mixed into the boundary layer, so the fluorescence gives a qualitative indication of the boundary layer thickness. At the left side of both images the boundary layer is visualized. At a higher angle of attack, the oblique shock on the flat plate is weaker and therefore the gas pressure is lower, resulting in a thicker boundary layer. This effect is observed in the images.

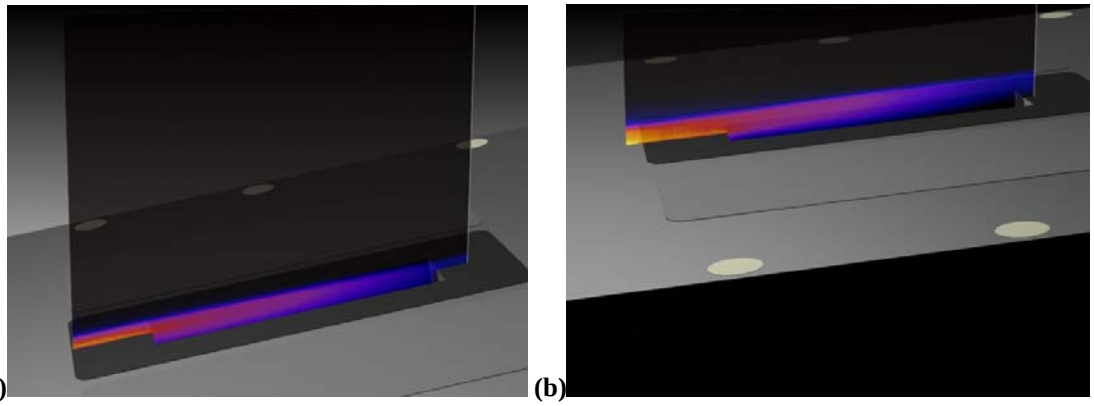

Figure 4: ViDI rendering of the flat plate / cavity flow experiment: close-up view for (a) 0° sting AoA (-10° flat plate AoA) and (b) 5° sting AoA (-5° flat plate AoA). The position of the virtual camera used to render this view was kept constant.

Figure 4 shows how the boundary layer dips into the cavity at the -10° flat plate AoA but the boundary layer skips somewhat over the cavity at -5°. Also the flow is notably smooth in the cavity: no expansion or shock waves are observed, even at the forward facing step at the right hand side of the cavity. It is possible that if more temperature-sensitive NO transitions had been probed with PLIF, additional detail might have been observed. However, the boundary layer is subsonic so it isn't necessarily expected to observe shockwaves and expansions in this flow which has a non-negligible boundary layer thickness.

(3) 70° Blunted Cone with Cylindrical Afterbody

During the early 1990's, a subgroup of the Advisory Group for Aerospace Research and Development (AGARD) fluid dynamics panel (Working Group 18) met to address several hypersonic flight issues, including blunt body near-wake flows.[24] The panel selected the wake flow behind a 70° blunted cone model with a cylindrical afterbody as a test case for investigation because of its relevance to Mars entry. This shape was tested in both real gas and perfect gas facilities (see Reference 25 and references therein). In addition to studying the influence of real gas effects on the wake flow, the reattachment process of a free shear layer was investigated. The working group realized that shear layer transition to turbulence would directly influence the near-wake flowfield, and in particular, the heat transfer associated with reattachment.[25] Prior work had indicated that impinging transitional shear layers could exhibit much higher peak heating than either fully laminar or fully turbulent shear layers.[25]

PLIF had previously been used to identify transition in underexpanded free jets for the Space Shuttle Return to Flight Program.[26] Thus, a few runs were performed in the Mach 10 Air wind tunnel to demonstrate that transition from laminar to turbulent flow could also be identified in the tunnel using PLIF. One area of particular interest was wake flows on entry capsules where hotwire probes are sometimes used to survey the wake flow to determine if the flowfield is laminar, transitional or turbulent.[27] Such hotwire probe surveys are very time consuming, sometimes taking many tunnel runs two days to complete for one angle of attack, since the probe must be scanned through many different positions relative to the model to sample the flowfield. Schlieren can also be used to visualize turbulence in wake flows, but at lower pressure conditions the results can be inconclusive: if turbulent structures are not observed with schlieren the flow may be laminar or the sensitivity may just be too low to see the turbulence. It was hoped that PLIF could confidently identify the wake flow behavior in single images.

The flow was seeded with pure NO at 0.1 slpm at a single point near the base of the model using a porous plug attached to a slender tube. A porous plug was used so that the velocity of the NO exiting the tube would be negligible and would not perturb the flow. The single shot image shown in Figure 5(a) clearly delineates the gas within the separated flow, marked by NO, and the shear layer, which marks the interface between NO-seeded

separated flow and non-seeded gas outside. The reattachment point (defined as the point of minimum width of the wake) is also clearly visualized. The shear layer is seen to be laminar near the separation point and transitions to turbulence further downstream, achieving vigorous turbulence near the reattachment point. Thus, PLIF was able to suitably visualize the state of the wake shear layer.

Upon closer inspection, several artifacts of the experiment are observed. The model had a 6-inch (22.9 mm) long quartz insert so that the laser sheet could penetrate through the cylindrical sting. Consequently the images show fluorescence both above and below the sting for much of the wake flow. The laser sheet was expanded to 11 inches (280 mm) wide to visualize the reattachment process towards the right of the image. So, beyond the extent of the quartz insert, the solid sting blocks the laser sheet, preventing fluorescence from being observed below. A small shadow is also observed below the sting just downstream of the base of the model. This shadow is caused by a piece of high-temperature tape wrapped around the sting, covering the window, This tape was used to secure the tube attached to the porous plug that seeded NO into the flow. The porous plug was placed on the opposite side of the model from the camera. So, it is not in the field of view of the laser sheet, nor does it appear in the ViDI renderings.

The PLIF intensity varies substantially from left to right in the images, peaking near the center. This is likely caused by a known variation in intensity in the laser sheet as well as some left-to-right spectral variation in the laser sheet. The images were not fully corrected to remove these nonuniformities, so the bright fluorescence in the center of the image is probably not fluid mechanically significant. Other than this left-to-right variation, the PLIF intensity is more continuous and uniform within the separated flow region than was anticipated, since the NO was seeded in at nearly a single point source less than 1 cm^3. In some other configurations similarly studied, the seeded NO approximately traced out streamtubes or streaks across the images. The uniformity of NO in Fig. 5 indicates that the gas in the separated flow region has a long residence time: NO has been distributed throughout the separated region.

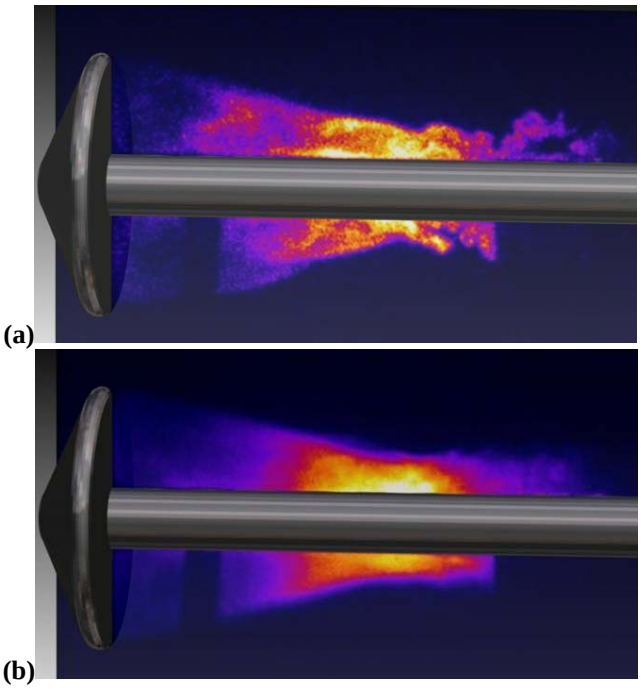

Figure 5: Wake flow behind the 70 degree blunted cone with a cylindrical afterbody at Mach 10 and P_0 = 10.0 MPa (1450 psia) . Top image (a) is a single shot while the bottom image (b) is an average of 100-single shots.

There is a slight asymmetry near the attachment point in both single-shot and averaged images: the width of the wake at the attachment point on the top half of the image is thicker than at the bottom. This could possibly indicate that the model was not perfectly aligned with zero degree angle of attack. However, this same effect could also be caused by or exacerbated by uncorrected lens distortions or by incorrect scaling and/or placement of the PLIF images over the computer rendered model during ViDI processing. In the next set of experiments, not reported here, care was taken to image a card displaying a regular pattern which was attached to the model and injected into the plane of the laser sheet prior to each experiment. These so-called "dot card images" allow distortion corrections to be applied as well as allowing precise determination of scale and placement of the images relative to the rendered models. This point is discussed in greater detail in Reference 3.

(4) Apollo Capsule

The Apollo-geometry capsule tests consisted of RCS-jet testing and a series of experiments to compare methods of seeding NO into the flow. While it was not desired to perturb the flowfield with the seed gas, some interesting effects were caused by flow seeding and these are also described below. This section includes (a) a summary of the RCS jet visualization results, (b) results from seeding and visualizing the shear layer on the leeward separated wake flow, (c) results from seeding the wake flow using a porous plug in the model, and (d) results from seeding the wake flow by using a tube attached to the exterior of the sting.

(4a) RCS Jet Visualizations

Figure 6 shows a ViDI rendering of the capsule model with a single-shot false-color NO PLIF image overlaid.[3] For this measurement, the laser sheet entered the flowfield from the top, was oriented parallel to the sting and was on the model centerline. The composition of the jet gas by mass was 95% nitrogen (N_2) and 5% nitric oxide (NO). PLIF was used to visualize the NO in the jet. The camera was placed at a right angle to the laser sheet. The flow is ejected normal to the surface and forms into an underexpanded jet. The nearfield flow consists of a barrel shock and Mach disk. As the flow continues downstream, it impinges on the shear layer bordering the separated flow region downstream of the capsule (this claim is substantiated by comparing with the shear layer visualizations in the next section). The shear layer bends the RCS jet and the jet propagates downstream.

During these tests, the RCS jet flow rate was varied between zero and 0.5 standard liters per minute and the angle of attack and tunnel stagnation pressure were also varied. In all cases, the RCS jets appeared to be laminar although slightly unsteady. Some of the flow visualization images were processed to determine the trajectory and to quantify the flapping of the RCS jet. The spatial resolution of the jet trajectory measurement was about 1 mm and the single-shot precision of the measurement was estimated to be 0.02 mm in the far field of the jet plume. The jet flapping, measured by the standard deviation of the jet centerline position was as large as 0.9 mm, while the jet was 1.5-4 mm in diameter (full width at half maximum). Schlieren flow visualization images were obtained for comparison with the PLIF results. Surface pressures were also measured and presented.[3]

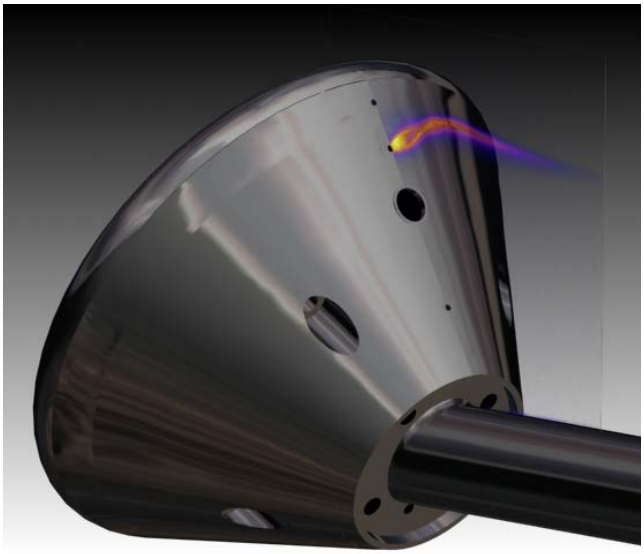

Figure 6: ViDI rendering of the capsule model with PLIF visualization of the RCS jet.[3] The virtual camera in ViDI has been oriented above the model and at a 45° angle to better show details of the model, such as the location of the RCS jet port and the relative size and location of the 0.25-in. diameter porous plug which is just below the RCS jet.

(4b) Shear layer visualization

Visualizing the location and the state (laminar, transitional or turbulent) of the shear layer forming at the upper edge of the separated flow downstream of the capsule has implications for both aerodynamics and aeroheating. One forebody pressure port / NO seed port (#5 in Reference 3) was used in several runs to seed the shear layer. The flowrate was adjusted between 0 and 0.5 slpm of a 5% NO / 95% N_2 gas mixture, and two different stagnation pressures (2.41 MPa (350 psia) and 4.96 MPa (720 psia)) were tested. The results are shown in Figure 7. Figure 7(a) shows a single shot image with P_0 = 2.41 MPa (350 psia) and the mass flow rate equal to 0.5 slpm. All such images showed turbulent flow. Note that in this and many similar images, the flow is becoming unsteady even on the forebody heatshield. The fluorescence drops off significantly on the right edge of the image because the laser sheet intensity was very low there. After this run, the laser sheet and camera were reoriented to better visualize the downstream flow. A test with the same flow rate but a higher stagnation pressure condition, shown in Figure 7(b), similarly showed turbulent flow. However, these visualizations repeatedly showed a nearly laminar flow on the bottom half of the shear layer while the top half of the shear layer appears turbulent, often with wisps of gas being generated nearly perpendicular to the shear layer by the seeded jet. Perhaps for these conditions, a vortex shedding process occurs from the injected gas jet, resulting in pulsations in the shear layer. However, when the flow rate of NO was decreased to 0.1 slpm, the flow became laminar, as shown in Figure 7(c) which was obtained at P_0 = 4.96 MPa (720 psia), (the higher Reynolds number condition of the two tested while seeding this port). Thus, the shear layer could be visualized with NO-seeded PLIF without forcing transition.

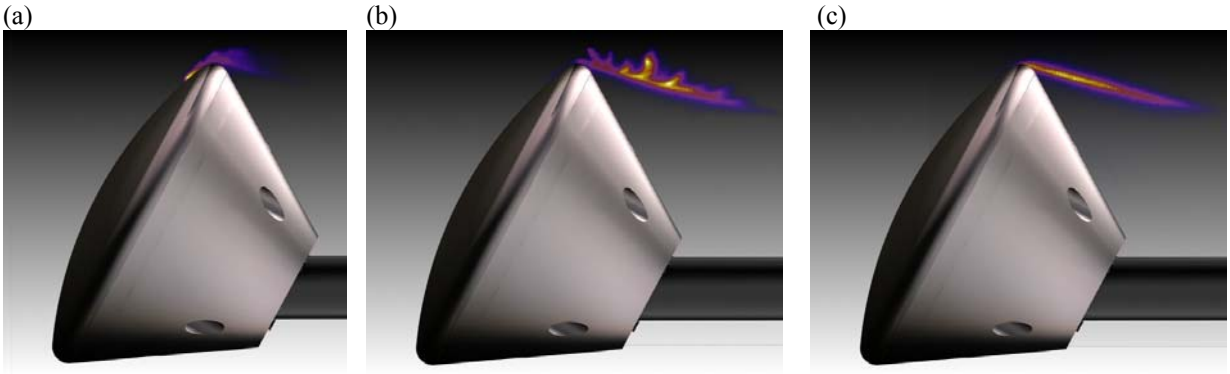

Figure 7: Visualization of the shear layer by flowing a 5% NO, 95% N2 gas mixture through port #5. Flow rates and stagnation pressures for these images were (a) $\dot{m}$ = 0.5 slpm, P_0 = 2.41 MPa (350 psia), (b) $\dot{m}$ = 0.5 slpm, P_0 = 4.96 MPa (720 psia), and (c) $\dot{m}$ = 0.1 slpm, P_0 = 4.96 MPa (720) psia.

(4c) Seeding from the porous plug.

One stainless steel tube supplied NO to a 0.25-in. (6.35-mm) diameter porous plug located just below the RCS jet, shown in Fig. 6. Seeding through the porous plug resulted in nearly 20 times lower velocity of the injected gas for a given flowrate, compared to a typical small-diameter pressure port. It was thought that lower gas velocity would perturb the flow less. The resulting images are shown in Figure 8. In Fig. 8(a) the mass flow rate was less than 0.05 slpm of pure NO and the fluorescence merely makes a glow around the port. When the flow rate is increased to 0.1 slpm, the NO penetrates deeper into the flow. The velocity of the gas exiting the porous plug is estimated to be about 10-15 meters per second at 0.1 slpm. So, it was anticipated that this low velocity gas would quickly be swept up in the crossflow. However, the fact that it penetrates deep into the flow (particularly in Fig. 8(c)) indicates that the flow velocity parallel to the models surface is even slower. The flow velocity at the surface appears to be towards the forebody/aftbody junction. When the NO finally reaches this rounded junction, it becomes highly stretched as it marks the shear layer and passes downstream. Note that the images shown are all averages over 100 single-shot images. However, the single shot images look very similar and all appear to be laminar, though the plume of NO shifts slightly from image to image showing a degree of unsteadiness. Importantly, this seeding location failed to distribute NO uniformly throughout the separated flow, as desired.

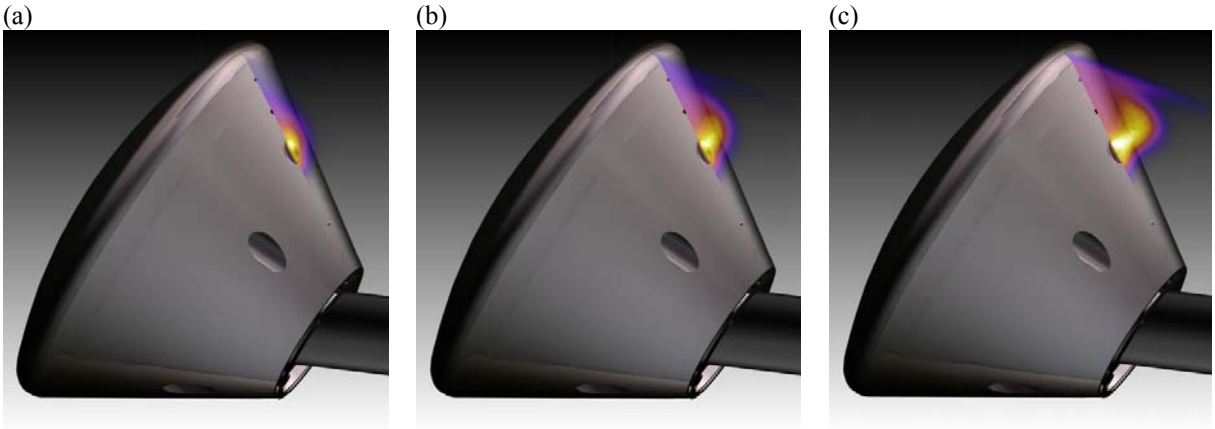

Figure 8: Visualization of pure NO seeded from the porous plug for (a) $\dot{m}$ < 0.05 slpm, (b) $\dot{m}$ = 0.1 slpm and (c) $\dot{m}$ = 0.2 slpm. The stagnation pressure was P_0 = 4.96 MPa (720 psia).

(4d) Seeding from a tube attached to the exterior of the sting.

Following the tests shown in Figure 8, it was desired to provide a high mass flow rate, low-velocity source of NO further aft of the model so that the NO would be entrained in the reverse separated flow, thereby providing visualization throughout the separated flow region. A quick solution was adopted: a 1/8-inch (3.2 mm) diameter tube was taped to the sting to supply NO near the sting/model junction. Initially, the end of the tube was cut at a 45 degree angle to supply the NO. The resulting flow showed a jet of NO-seeded N_2 exiting the tube. This jet clearly perturbed the wake flow. To lessen the perturbations, the tube was then closed at the end and 10-15 small diameter holes were drilled in the tube at random to allow the NO to exit the tube at low velocity in many directions, thereby preventing a large coherent jet. The end of the tube was placed very close to the sting/model junction. An example image resulting from this arrangement is shown, rendered with ViDI, in Figure 9(a). In this and all images, the laser was oriented parallel to the flow direction and entered from the top. The fluorescence is brightest just above the seeding tube.

To systematically obtain measurements at locations in the flow other than the model centerline, the laser sheet was swept spanwise through the flow. The laser was still impinging on the model from above and the width of the laser sheet was still parallel to the axis of the sting and the tunnel. However, the sheet no longer coincided with the centerline of the model. It was initially placed close to the model centerline and was swept away from the camera at a rate of 6.5 mm/s. In 10 seconds, at a frame rate of 10 Hz, the three dimensional flowfield above the sting was sampled. In post-processing, these one hundred 512- x 512-pixel images were converted into five hundred and twelve 100-x 512-pixel composite images. Figure 9(b) shows smoothed 100-x 512-pixel images overlaid on the model. These images show the evolution of the shape of the wake flow as it propagates downstream. The wake vortex pattern is observed to form an upright half-mushroom shaped flow at least for the conditions measured here. Only half of the wake is shown because the laser sheet could not be scanned towards the camera further than the model centerline because the laser directly reflected towards the camera, potentially damaging the image intensifier. We have overcome this problem in subsequent experimentation by changing the orientation of the camera and by using additional spectral filtering.

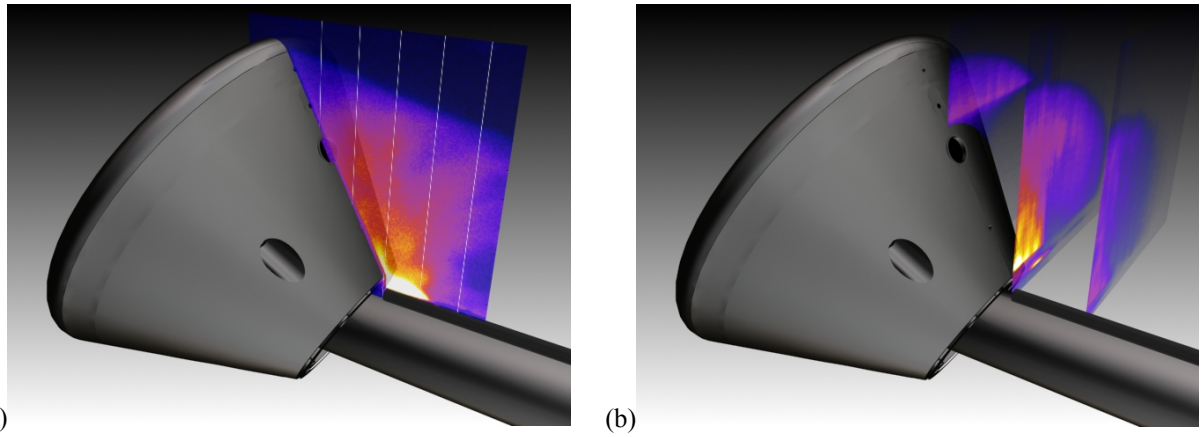

(a) (b)

Figure 9: Visualization of pure NO seeded from a 3.2 mm diameter tube (shown on the top of the sting in black) containing multiple drilled holes. Image (a) is the average of two single-shot streamwise images while (b) shows computer generated spanwise images at three different downstream locations. The white vertical lines in (a) indicate where 5 different spanwise planes of data were reconstructed, 3 of which are shown in (b).

V. Conclusion

The planar laser-induced fluorescence technique has been applied to study four different hypersonic flowfields. The wake vortex on the leeward side of a fuselage-only X-33 model was visualized. An interesting behavior was observed at high angles of attack where the vortex switched from a symmetric to an asymmetric mode. The boundary layer on a flat plate was visualized as it passed into or over an open rectangular cavity, depending on the conditions tested. The wake flow behind a 70 degree blunted cone with a cylindrical afterbody was visualized: laminar-to-turbulent transition was identified by examining single images. Finally, an Apollo-geometry entry capsule was tested. An RCS jet was visualized as was the shear layer at the edge of the separated wake flow. Two different schemes were successfully used to seed more of the wake flowfield and one of these methods allowed

spanwise images of the wake flow to be generated and displayed. In this paper, PLIF was only used for flow visualization. However, the method can also provide quantitative measurements of parameters like velocity and temperature. In future work we will explore the use of these measurement methods for studying hypersonic flows.

Acknowledgments

We wish to acknowledge the contribution to this project from the NASA Langley Research Center 31-Inch Mach 10 Air tunnel technicians and engineers, including Kevin Hollingsworth, Rhonda Murphy, Henry Fitzgerald, Johnny Ellis and Paul Tucker. We also wish to acknowledge Jeff Balla and Tom Horvath at NASA Langley Research Center for providing the AGARD planetary entry model. The Apollo model was designed for this test by Greg Brauckmann and Vince LeBoffe. Finally, we wish to acknowledge Bob Nowak for suggesting the use of and providing the X-33 model and Joel Everhart for providing the flat-plate/cavity flow model.

References

[1] L. M. Weinstein, "An improved large-field focusing schlieren system," AIAA-1991-567, *29th Aerospace Sciences Meeting,* Reno, NV, Jan. 7-10, 1991.

[2] B. Shirinzadeh, R.J. Balla, and M.E. Hillard, "Rayleigh scattering measurements in supersonic facilities," AIAA-96-2187, 19th AIAA Advanced Measurement and Ground Testing Technology Conference, New Orleans, LA, June 1996.

[3] P.M. Danehy, J. Wilkes, G. Brauckmann, D. Alderfer and S. Jones, D. Patry, "Visualization of a Capsule Entry Vehicle Reaction-Control System (RCS) Thruster," AIAA-2006-1532 44th AIAA Aerospace Sciences Meeting and Exhibit, Reno, Nevada, Jan. 9-12, 2006.

[4] P.H. Paul, M.P. Lee, R.K. Hanson, Molecular velocity imagining of supersonic flows using pulsed planar laser-induced fluorescence of NO, Opt. Lett., Vol. 14, 417-419, 1989.

[5] B.K. McMillin, J. L. Palmer and R.K. Hanson, "Temporally resolved, two-line fluorescence imaging of NO in a transverse jet in a supersonic cross-flow," Appl. Opt., 32, 7532, 1993.

[6] W. L. Roberts, M. G. Allen, R. P. Howard, G. J. Wilson, R. Trucco, "Measurement and Prediction of Nitric Oxide Concentration in the HYPULSE Expansion Tube Facility," AIAA 94-2644, 1994.

[7] W.M. Ruyten, M.S. Smith and L.L. Price, "Status of Laser-Induced Fluorescence and Planar Laser Induced Fluorescence Measurements in the AEDC HEAT-H2 Arc Heater Facility" AIAA 95-2038, 1995.

[8] W. M. Ruyten "Comparison of calculated and measured temperature fields in the AEDC Impulse Facility" AIAA-1996-2237, 1996.

[9] A.F.P. Houwing, J. L. Palmer, M. C. Thurber, S. D. Wehe, R. K. Hanson, R. R. Boyce, "Comparison of planar fluorescence measurements and computational modeling of a shock layer flow," AIAA Journal, Vol. 34 (3), 470-477, 1996.

[10] W. H. Beck, G. Eitelberg, O. Trinks, and M. Wollenhaupt, "Testing methodologies in the DLR High Enthalpy Shock Tunnel HEG," AIAA-1998-2770, 1998.

[11] J. S. Fox, A. F. P. Houwing, P. M. Danehy, M. J. Gaston, N. R. Mudford, S. L. Gai, "Mole-Fraction-Sensitive Imaging of Hypermixing Shear Layers," Journal of Propulsion and Power, Journal of Propulsion and Power, 17(2), p. 284-292, 2001.

[12] P. C. Palma, P. M. Danehy, A. F. P. Houwing, "Fluorescence Imaging of Rotational and Vibrational Temperature in a Shock Tunnel Nozzle Flow," AIAA Journal, Vol. 41, no. 9, Sept. p. 1722-1732, 2003.

[13] R. J. Exton, R. J. Balla, B. Shirinzadeh, M. E. Hillard, and G. J. Brauckmann, "Wake imaging in supersonic facilities using the iodine Cordes bands," AIAA-1998-2697, 1998.

[14] J. McDaniel, C. Glass, D. Staack, and C. Miller, "Experimental and Computational Comparison of an Underexpanded Jet Flowfield", AIAA Paper No. 2002-0305, January 2002.

[15] J. A. Wilkes, D. W. Alderfer, S. B. Jones, and P. M. Danehy, "Portable Fluorescence Imaging System for Hypersonic Flow Facilities," *JANNAF Interagency Propulsion Committee Meeting*, Colorado Springs, Colorado, December 2003.

[16] J. A. Wilkes, C.E. Glass, P.M. Danehy, and R.J. Nowak, "Fluorescence Imaging of Underexpanded Jets and Comparison with CFD", AIAA Paper No. 2006-0910, January 2006.

[17] B. R. Hollis, R. A. Thompson, S. A. Berry, T. J. Horvath, K. J. Murphy, R. J. Nowak, and S. J. Alter, "X-33 Computational Aeroheating/Aerodynamic Predictions and Comparisons With Experimental Data", NASA Technical Publication, NASA/TP-2003-212160, May 2003.

[18] K.J. Murphy "X-33 Hypersonic Aerodynamic Characteristics," Master's Thesis, The University of Texas at Austin, December, 2000.
[19] J. R. Micol "Langley Aerothermodynamic Facilities Complex: Enhancements and Testing Capabilities," AIAA Paper 98-0147, 36th AIAA Aerospace Sciences Meeting & Exhibit, January 12-15, Reno, NV, 1998.
[20] R. J. Schwartz, "ViDI: Virtual Diagnostics Interface Volume 1-The Future of Wind Tunnel Testing" Contractor Report NASA/CR-2003-212667, December 2003
[21] http://www.autodesk.com/
[22] S. O'Byrne, P. M. Danehy, A. F. P. Houwing, "PLIF temperature and velocity distributions in laminar hypersonic flat-plate flow" 20th International Congress on Instrumentation in Aerospace Simulation Facilities, August, 2003.
[23] J. L. Everhart, S. J. Alter, N. R. Merski, W. A. Wood, R. K. Prabhu, "Pressure Gradient Effects on Hypersonic Cavity Flow Heating" AIAA Paper 2006-0185, 2006.
[24] W. S. Saric, et al., Hypersonic Experimental and Computational Capability, Improvement and Validation. AGARD-AR-319 Vol 1., 1996.
[25] T. Horvath, K. Hannemann, "Blunt body near-wake flow field at Mach 10" AIAA Paper 97-0986, AIAA Aerospace Sciences Meeting & Exhibit, 35th, Reno, NV, Jan. 6-9, 1997.
[26] J. A. Wilkes, P. M. Danehy, and R. J. Nowak, "Fluorescence Imaging Study of Transition in Underexpanded Free Jets" 21st International Congress on Instrumentation in Aerospace Simulation Facilities, Sendai, Japan, Aug. 29-Sept. 1, 2005.
[27] T. J. Horvath, C. B. McGinley, and K. Hannemann, "Blunt Body Near Wake Flow Field at Mach 6," 27th Fluid Dynamics Conference, June 18-20, New Orleans, LA, AIAA 96-1935, 1996.